

## Supporting Information

# **Twin applications of highly selective Cu<sup>2+</sup> fluorescent Chemosensor and Cytotoxicity of 2-(2-phenylhydrazono)-1*H*-indene-1,3(2*H*)-dione and 2-(2-(4-methoxyphenyl)hydrazono)-1*H*-indene-1,3(2*H*)-dione and its Molecular docking and DFT Studies**

**Annamalai Subhasri<sup>a</sup>, Chinnadurai Anbuselvan<sup>a\*</sup> and Nagarajen Rajendraprasad<sup>b</sup>**

<sup>a</sup>*Department of Chemistry, Annamalai University, Annamalainagar – 608 002, India.*

<sup>b</sup>*Department of Biochemistry and Biotechnology, Annamalai University, Annamalai Nagar– 608 002, India.*

*\*Corresponding author email: [cas\\_amu@yahoo.co.in](mailto:cas_amu@yahoo.co.in)*

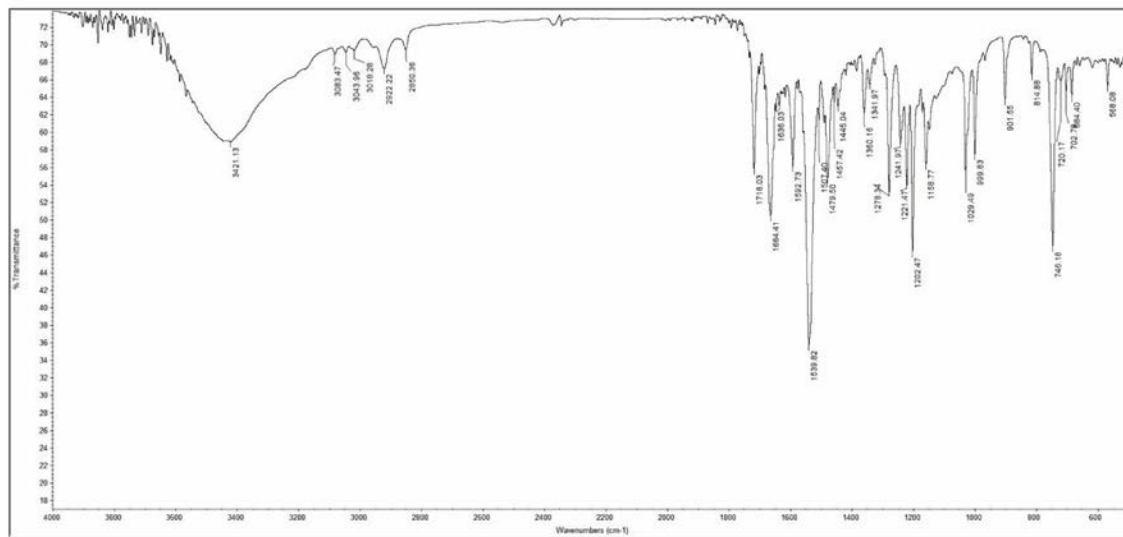


**Fig. S1** IR spectrum of compound (1)

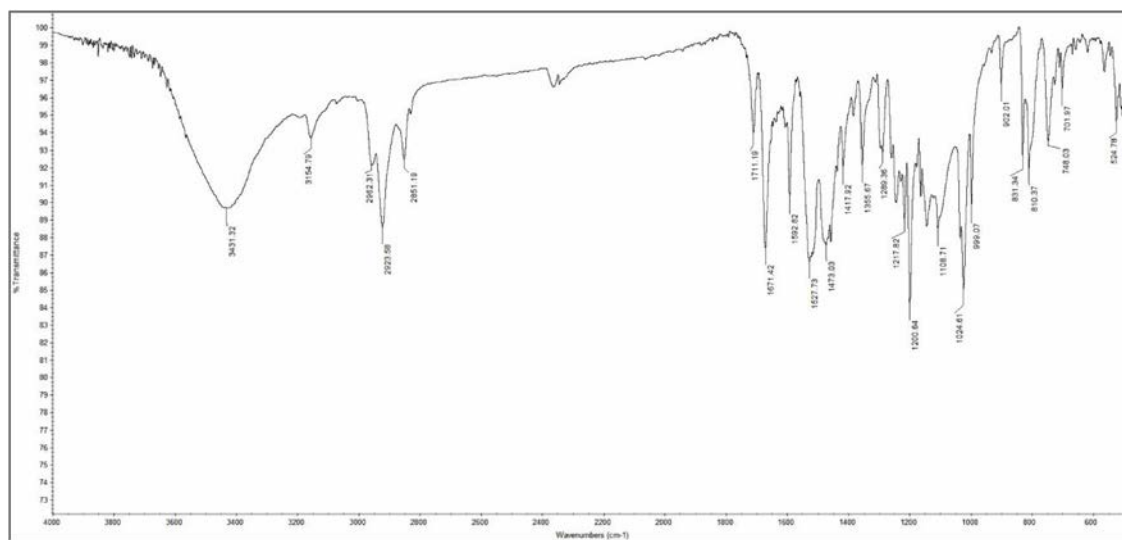


**Fig. S2** IR spectrum of compound (2)

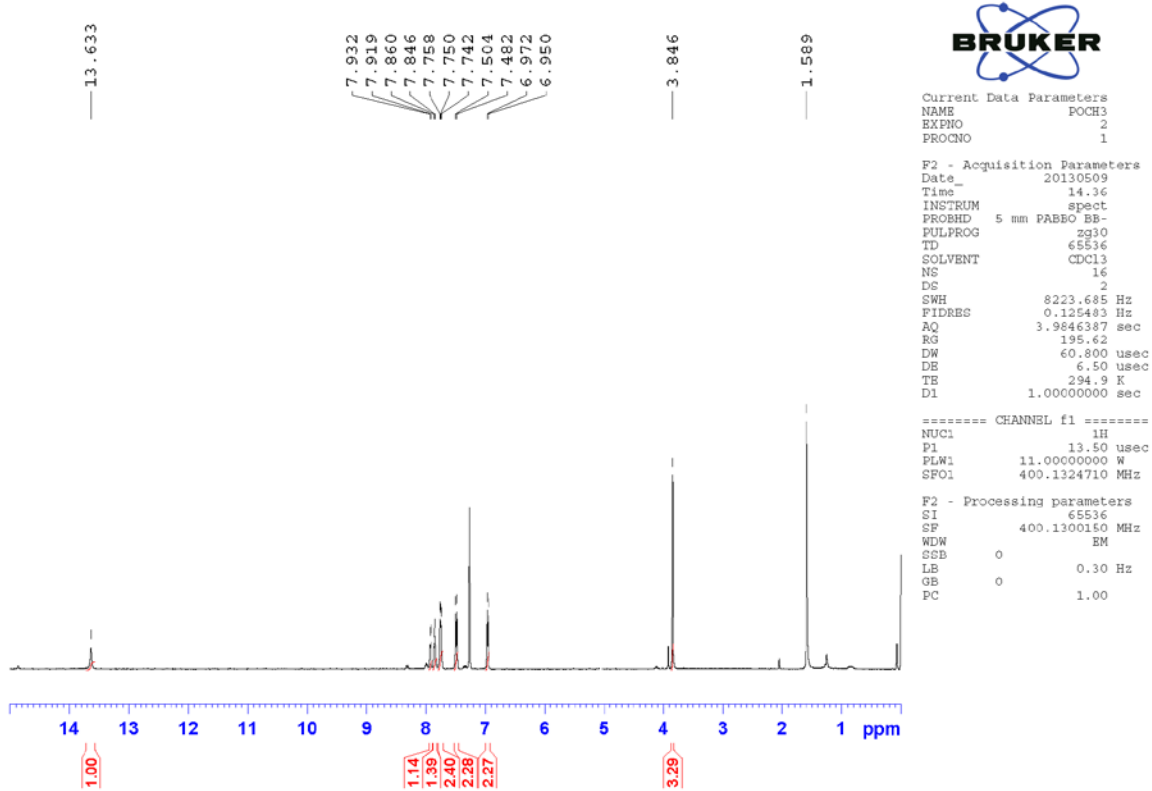
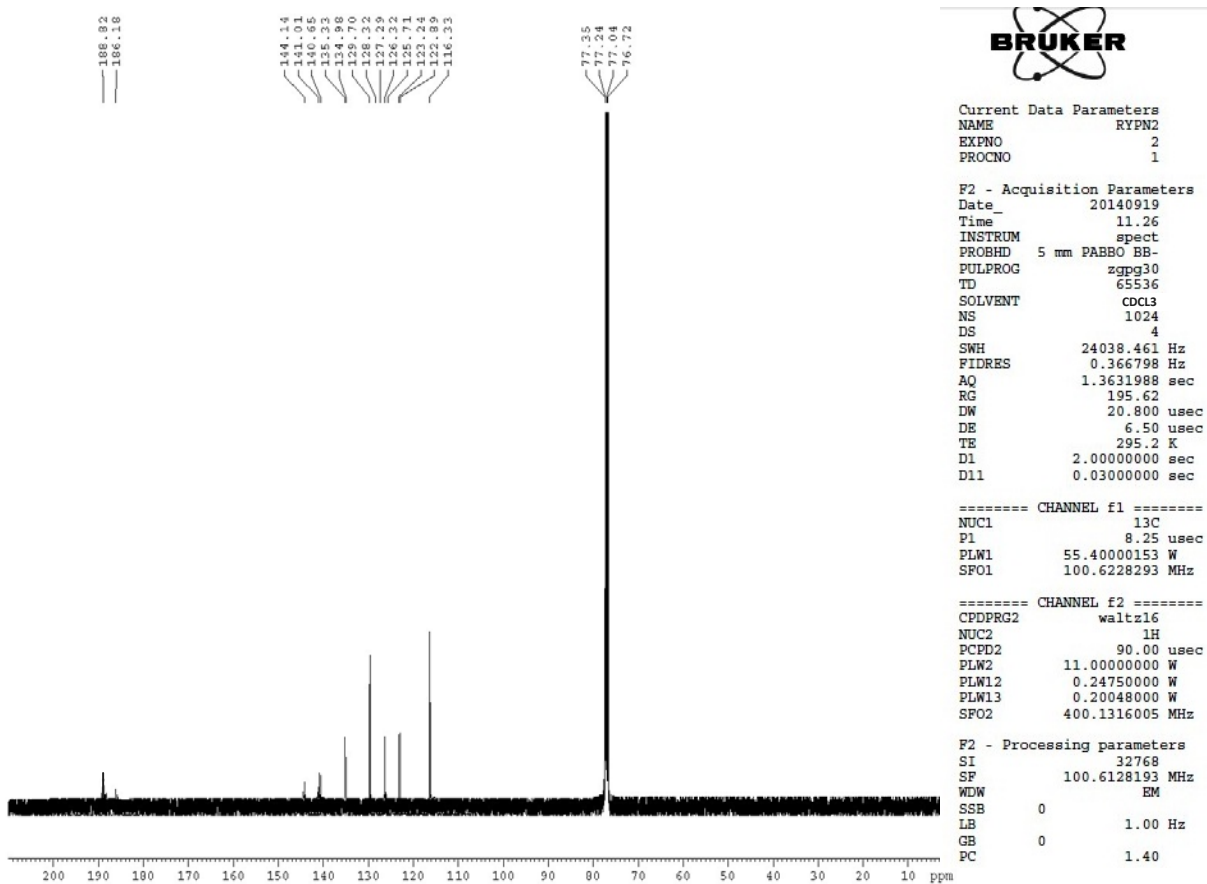


Fig. S3  $^1\text{H}$  NMR spectrum of compound (2)



**Fig. S4**  $^{13}\text{C}$  NMR spectrum of compound (1)

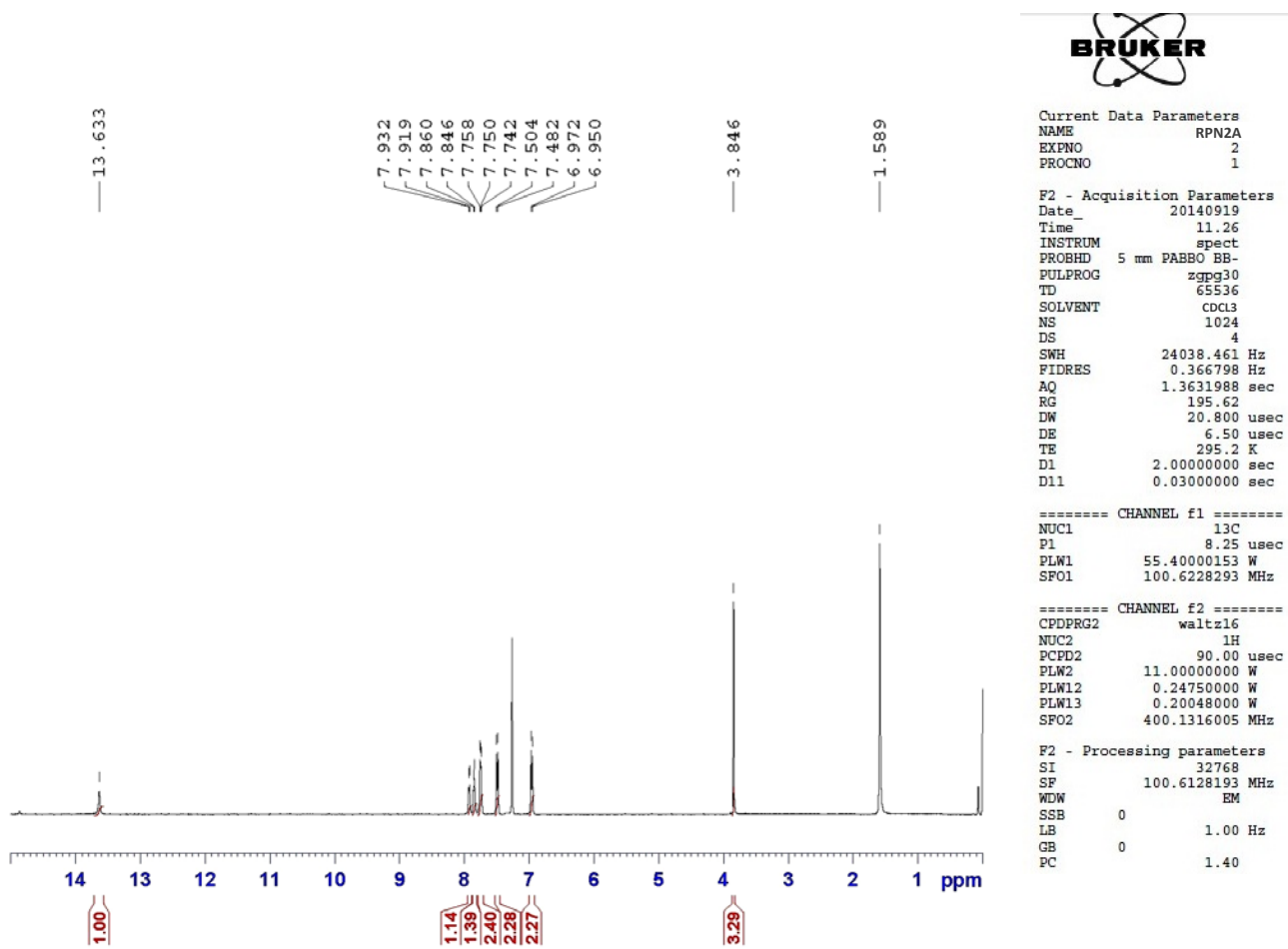
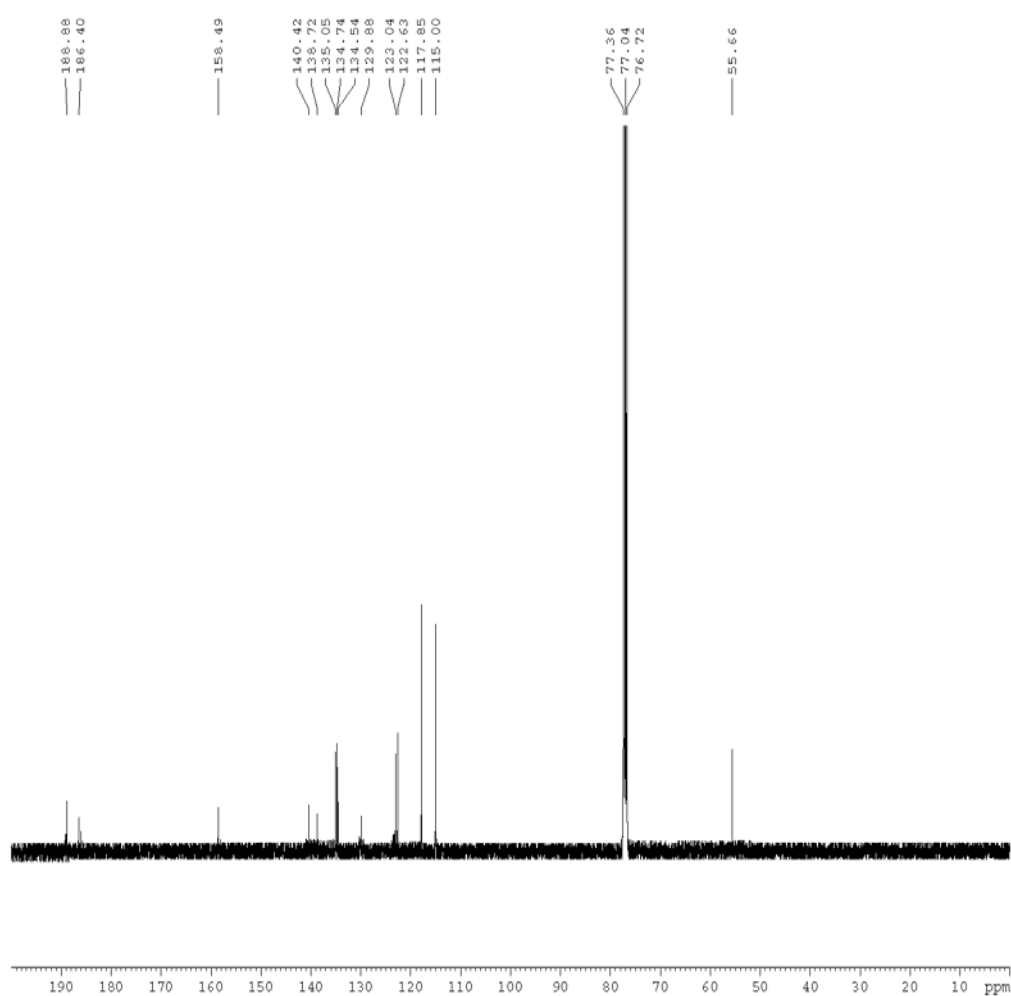


Fig. S5 <sup>1</sup>H NMR spectrum of compound (1)



```

Current Data Parameters
NAME                RPN2A
EXPNO                2
PROCNO              1

F2 - Acquisition Parameters
Date_               20140919
Time                11.26
INSTRUM             spect
PROBHD              5 mm PABBO BB-
PULPROG             zgpg30
TD                  65536
SOLVENT             CDCl3
NS                  1024
DS                   4
SWH                 24038.461 Hz
FIDRES              0.366798 Hz
AQ                  1.3631988 sec
RG                   195.62
DW                  20.800 usec
DE                   6.50 usec
TE                  295.2 K
D1                   2.00000000 sec
D11                  0.03000000 sec

===== CHANNEL f1 =====
NUC1                 13C
P1                    8.25 usec
PLW1                  55.40000153 W
SFO1                  100.6228293 MHz

===== CHANNEL f2 =====
CPDPRG2             waltz16
NUC2                  1H
PCPD2                 90.00 usec
PLW2                  11.00000000 W
PLW12                  0.24750000 W
PLW13                  0.20048000 W
SFO2                  400.1316005 MHz

F2 - Processing parameters
SI                    32768
SF                    100.6128193 MHz
WDW                    EM
SSB                    0
LB                      1.00 Hz
GB                      0
PC                      1.40

```

Fig. S6  $^{13}\text{C}$  NMR spectrum of compound (1)

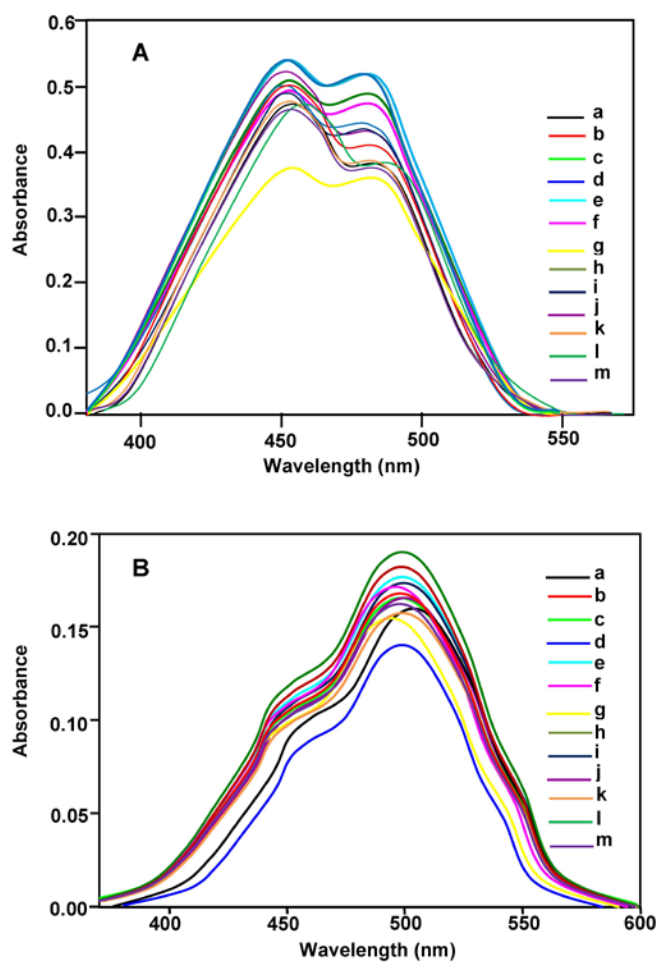


**Fig. S7** Absorbance spectrum of (A) compound (1) and (B) compound (2) with different solvents (a) 1,4-dioxane, (b) Acetonitrile, (c) Chloroform, (d) DMSO, (e) Ethanol, (f) 2-propanol, (g) Benzene, (h) Dichloromethane, (i) Ethylacetate, (j) Hexane, (k) 2-methylpropane1-ol, (l) Methanol and (m) 1-Hexanol.

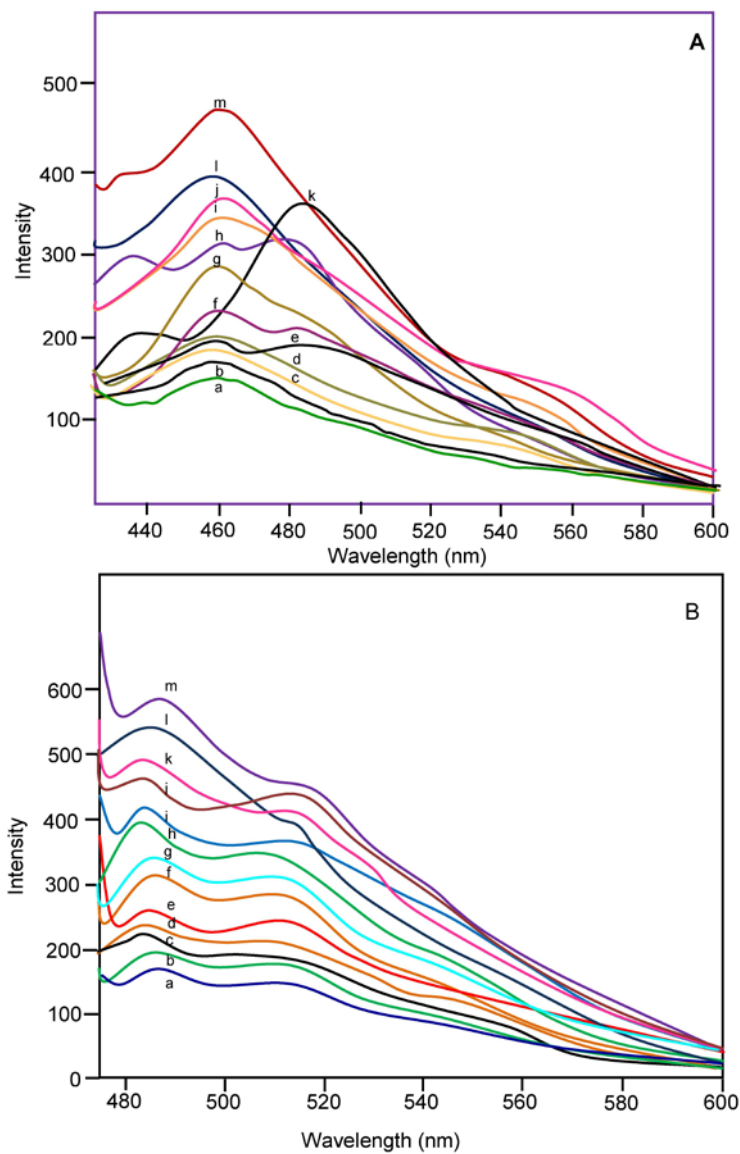


**Fig. S8** Emission spectra of compounds (1) and (2) with different solvents (a) 1,4-dioxane, (b) Acetonitrile, (c) Chloroform, (d) DMSO, (e) Ethanol, (f) 2-propanol, (g) benzene, (h) Dichloromethane, (i) Ethylacetate, (j) Hexane, (k) 2-Methylpropane-1-ol, (l) Methanol and (m) 1-Hexanol.

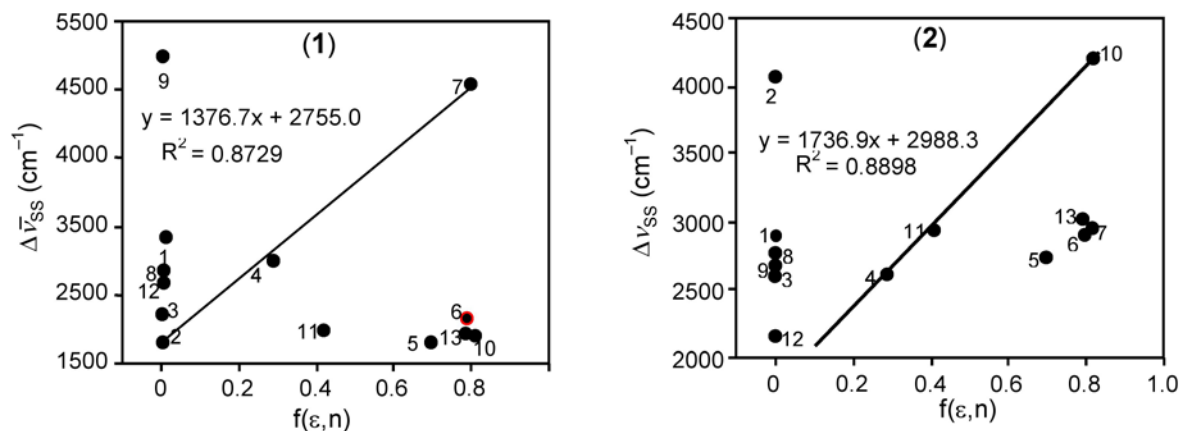


**Fig. S9** Plot of Stokes shifts ( $\text{cm}^{-1}$ ) Vs  $f(\epsilon,n)$  for compounds (1) and (2). 1. Hexane, 2. 1,4-dioxane, 3. benzene, 4. chloroform, 5. 2-propanal, 6. Ethanol, 7. Methanol, 8. 1.Hexanol, 9. 2-methylpropane-1-ol, 10. Acetonitrile, 11. Ethylacetate, 12. Dichloromethane, 13 . dimethylsulfoxide.

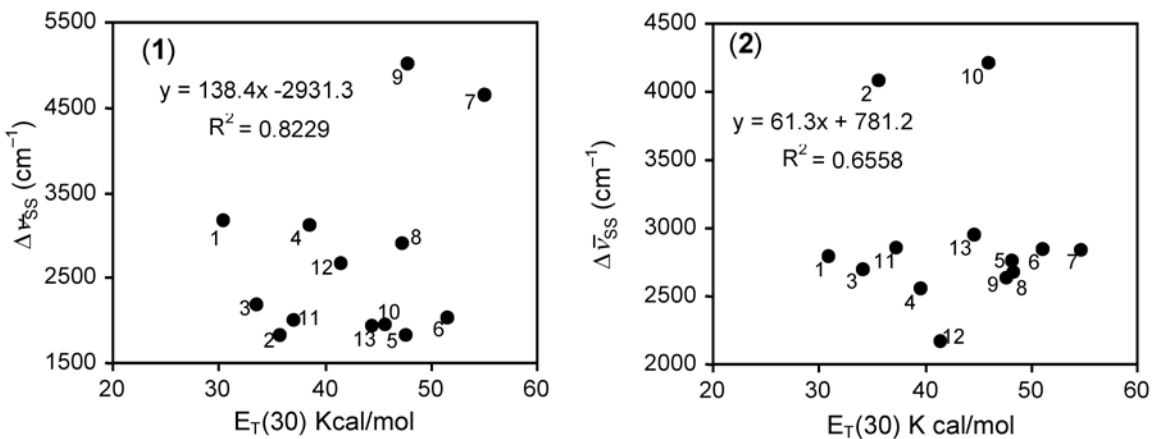


**Fig. S10.** Plot of Kawski correlation  $\bar{\nu}_a + \bar{\nu}_f$  ( $\text{cm}^{-1}$ ) Vs ET30 for compounds (1) and (2). 1. Hexane, 2.1,4-dioxane, 3. benzene, 4. chloroform, 5. 2-propanal, 6. Ethanol, 7. Methanol, 8. 1.Hexanol, 9. 2-methylpropane-1-ol, 10. Acetonitrile, 11. Ethyl acetate, 12.Dichloromethane, 13 . dimethylsulfoxide.

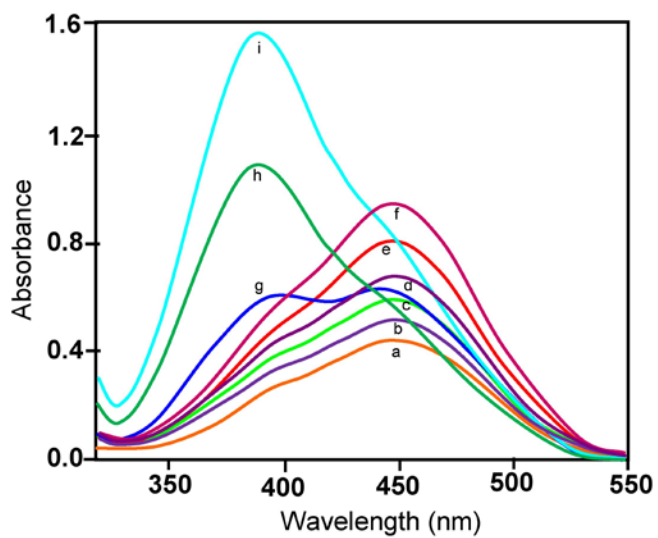
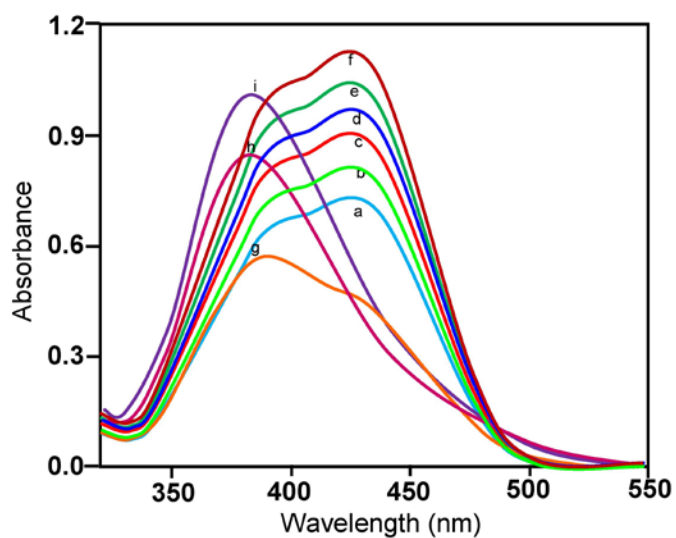


**Fig. S11** Absorbance spectra of compound (1) “a” and comound (2) “b” in ethanol:H<sub>2</sub>O with Cu<sup>2+</sup> Solution at different pH. (a-i) pH = 3 to pH = 11.

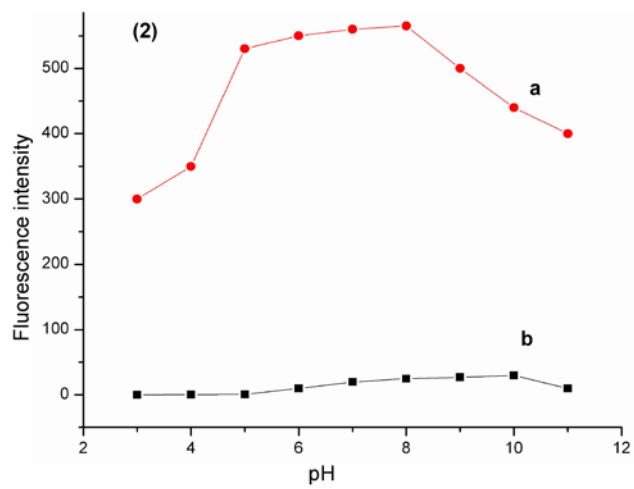
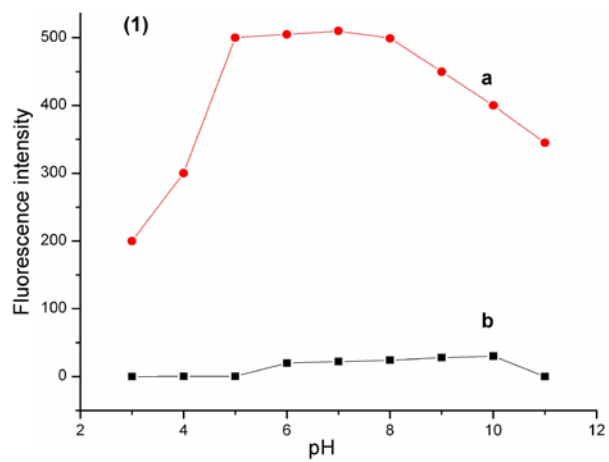


**Fig. S12** The effect of pH on the fluorescence intensity of compounds (1) and (2) (10  $\mu\text{M}$ ) in the bound (a) and the unbound (b) of 5 equiv. of  $\text{Cu}^{2+}$ .

**Estimation of Metal salts.** A stock solution of compound **(1)** ( $1.0 \times 10^{-3}$ ) and **(2)** ( $1.0 \times 10^{-3}$  M) were prepared in  $\text{CH}_3\text{CH}_2\text{OH}/\text{H}_2\text{O}$  (1:1, v/v). Solutions of  $2.0 \times 10^{-4}$  M salts of the respective cation were prepared in distilled water. All experiments were carried out in  $\text{CH}_3\text{CH}_2\text{OH}/\text{H}_2\text{O}$  solution ( $\text{CH}_3\text{CH}_2\text{OH}/\text{H}_2\text{O} = 1:1$ , v/v, 10  $\mu\text{M}$  HEPES buffer, pH = 7.0). In titration experiments, each time  $4 \times 10^{-5}$  M solution of **(1)** and **(2)** were filled in a quartz optical cell of 1 cm optical path length, and the ion stock solutions were added into the quartz optical cell gradually by using a micropipet. Spectral data were recorded at 1 min after the addition of the ions. In selectivity experiments, the test samples were prepared by placing appropriate amounts of the anions/cations stock into 2 mL of solution of **(1)** ( $1.0 \times 10^{-3}$ ) and **(2)** ( $1.0 \times 10^{-3}$  M).

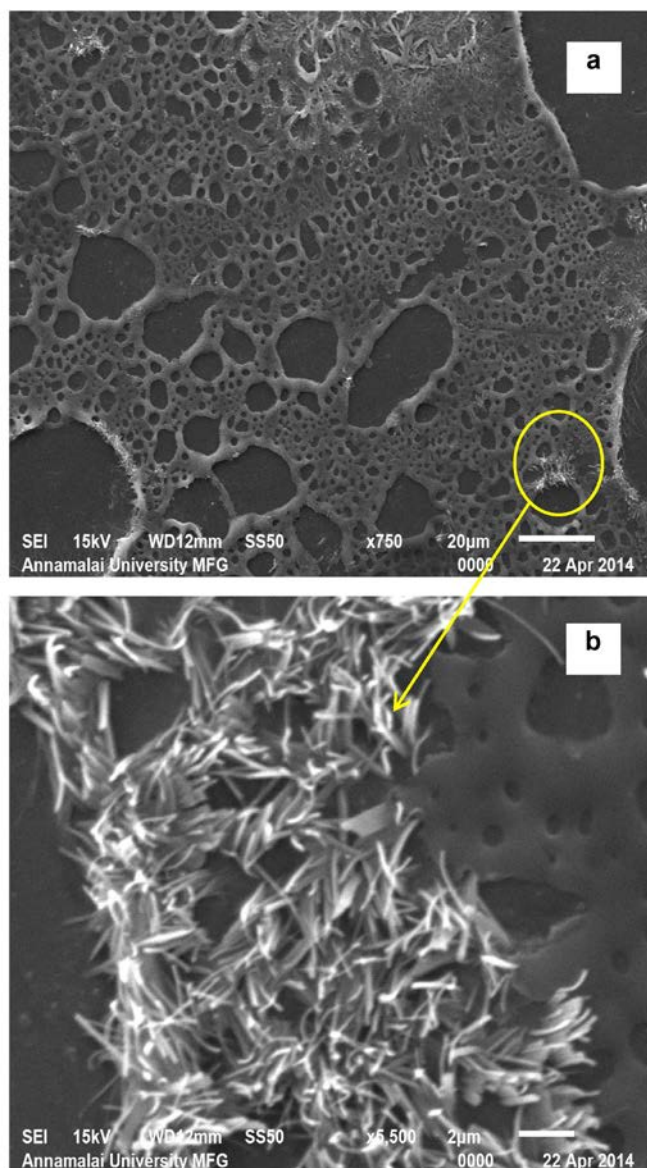


**Fig. S13** SEM images of compound (1) (a) 20  $\mu\text{m}$  and (b) 2  $\mu\text{m}$ .

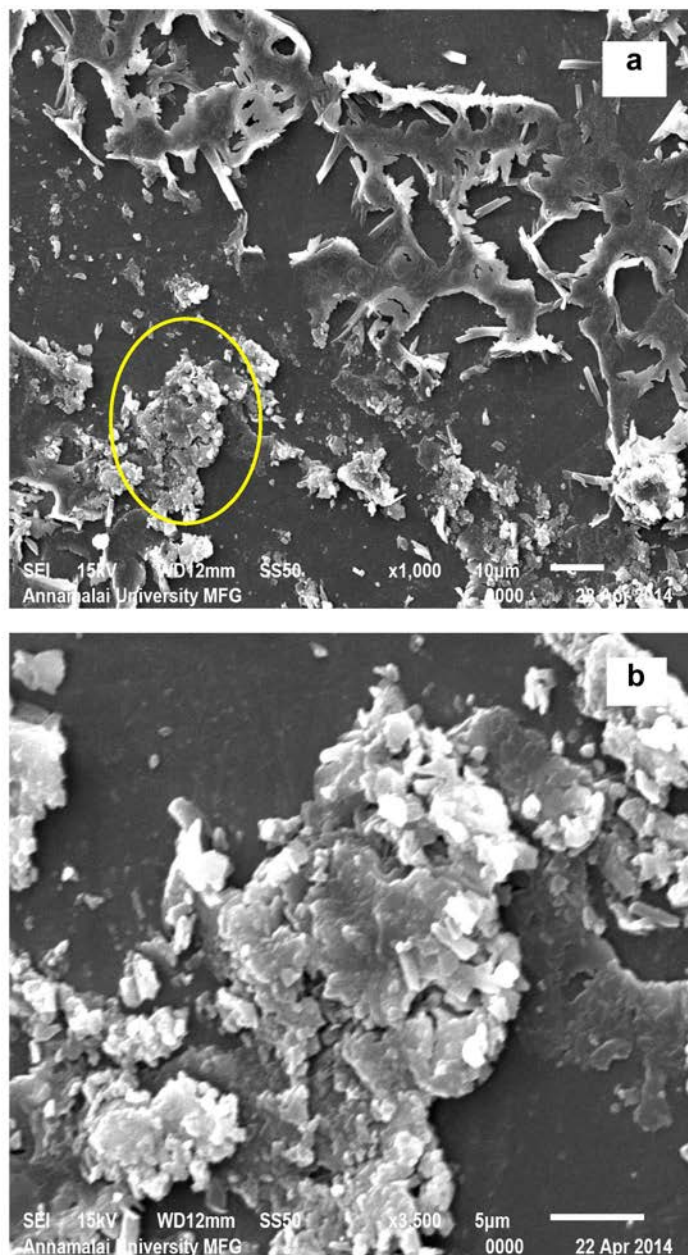


**Fig. S14** SEM images of complex  $\text{Cu}^{2+}$ -compound (1) (a) 10  $\mu\text{m}$  and (b) 5  $\mu\text{m}$ .

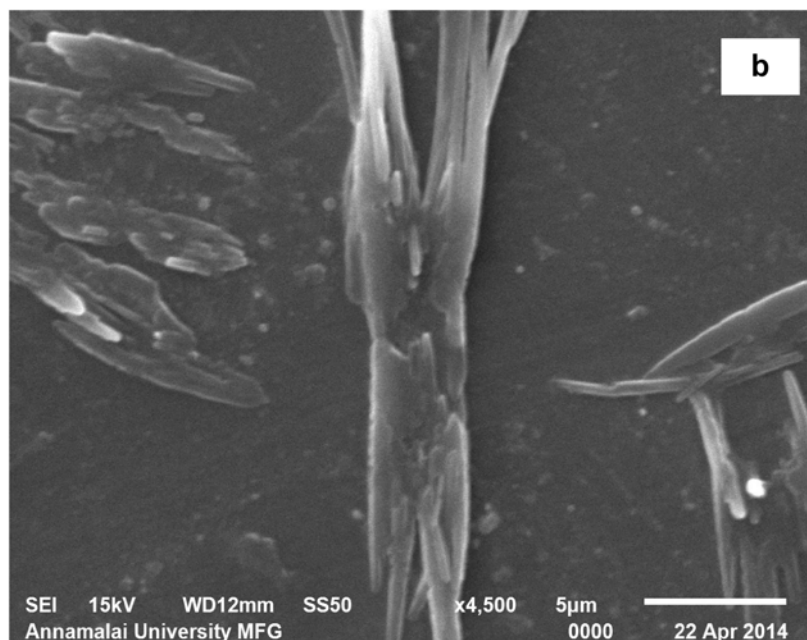
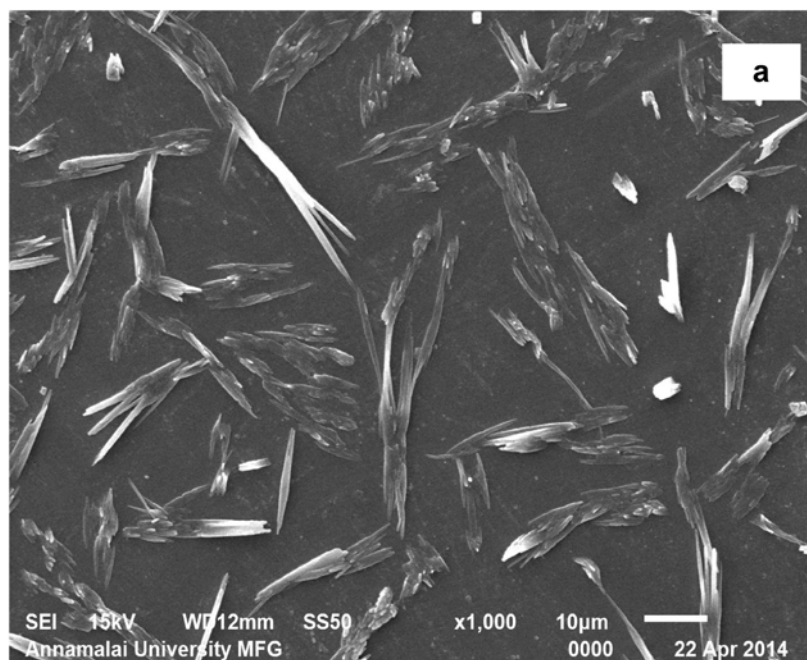


**Fig. S15** SEM images of compound (2) (a) 10 μm and (b) 5 μm.

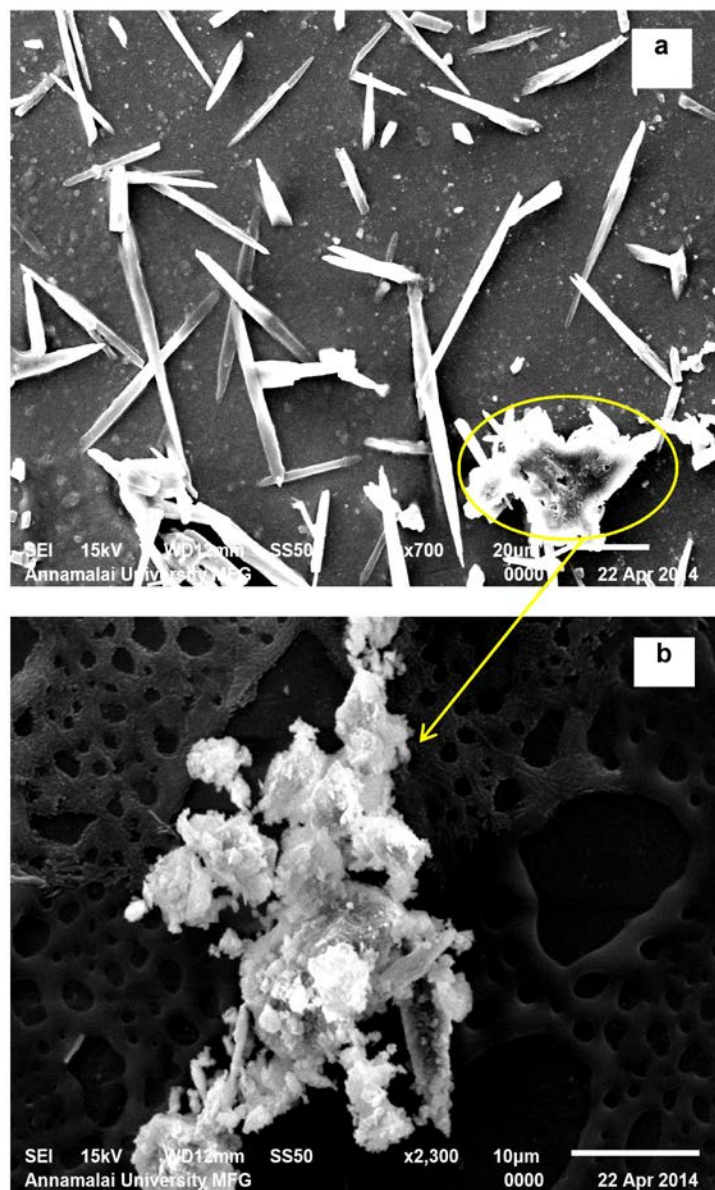


**Fig. S16** SEM images of complex  $\text{Cu}^{2+}$ -compound (2) (a) 20  $\mu\text{m}$  and (b) 10  $\mu\text{m}$ .

Scanning electron microscopy (SEM) was used to analyze the surface morphology of the microstructure of the resulting compounds **(1)**, **(2)** and its complexes with  $\text{Cu}^{2+}$ . Platinum was coated on the surface of compound **(1)** and images at 20 and 2  $\mu\text{m}$  are shown in Fig. S13a and b respectively. The ligand **(1)** shows a highly porous structure and grass like structure. The ligand **(2)** illustrated microrods like structure (Fig. S15a and b). We observed considerable change in the ligands morphology when cobalt ion was added to them (i.e. in the complex). The complex of **(1)** with  $\text{Cu}^{2+}$  ion, shows the grass covered with large amount spherical particles like surface morphology (Fig. S14a and b), but their size was relatively different. The complex of **(2)** with  $\text{Cu}^{2+}$  ion, shows self-assembled microsheets (Fig. S16a and b).

### **Molecular modeling: docking study**

Docking calculations were carried out by Docking Server.<sup>1</sup> Gasteiger partial charges were additional to the ligand atoms. Non-polar hydrogen atoms were merged, and rotatable bonds were defined. Necessary hydrogen atoms, Kollman united atom type charges, and solvation parameters were added with the aid of AutoDock tools.<sup>2</sup> Affinity (grid) maps of  $\times\times$  Å grid points and 0.375 Å spacing were generated using the Autogrid program.<sup>3</sup> AutoDock parameter set- and distance-dependent dielectric functions were used in the calculation of the van der Waals and the electrostatic terms, respectively. Docking simulations were performed using the Lamarckian genetic algorithm (LGA) and the Solis & Wets local search method.<sup>4</sup> Initial position, orientation, and torsions of the ligand molecules were set randomly. All rotatable torsions were released during docking. Each docking experiment was derived from 10 different runs that were set to terminate after a maximum of 250000 energy evaluations. The population size was set to 150. During the search, a translational step of 0.2 Å, and quaternion and torsion steps of 5 were applied.

The native structure of 4LRH, 4EKD, 4GIW and 4L9K are taken from the Protein Data Bank. Docking studies were performed with the online docking server, which utilizes the Lamarckian Genetic Algorithm (LGA) implemented therein. For the docking of the drug with 4LRH, 4EKD, 4GIW and 4L9K, the required file for the ligand (corresponding to the three-dimensional structure of the drug compound **(1)** and **(2)**) was created through the combined use of the Gaussian 03W and Docking Server. The geometry of compound **(1)** and **(2)** are first

optimized at the DFT B3LYP/6-31G level of theory using the Gaussian 03W suite of programs and the resultant geometry was read in the online docking server software in a compatible file format, from which the required file was generated in online docking server.

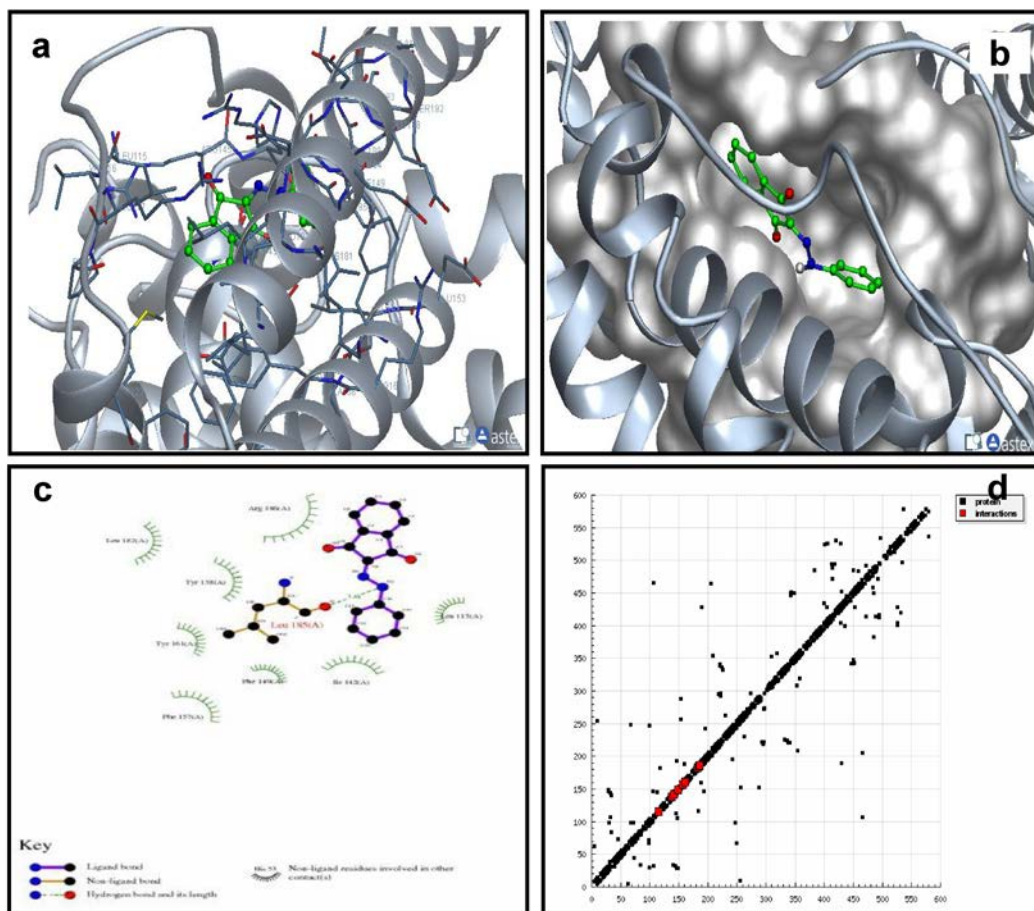


**Fig. S17** Molecular docking studies of compound (1) with 4L9K

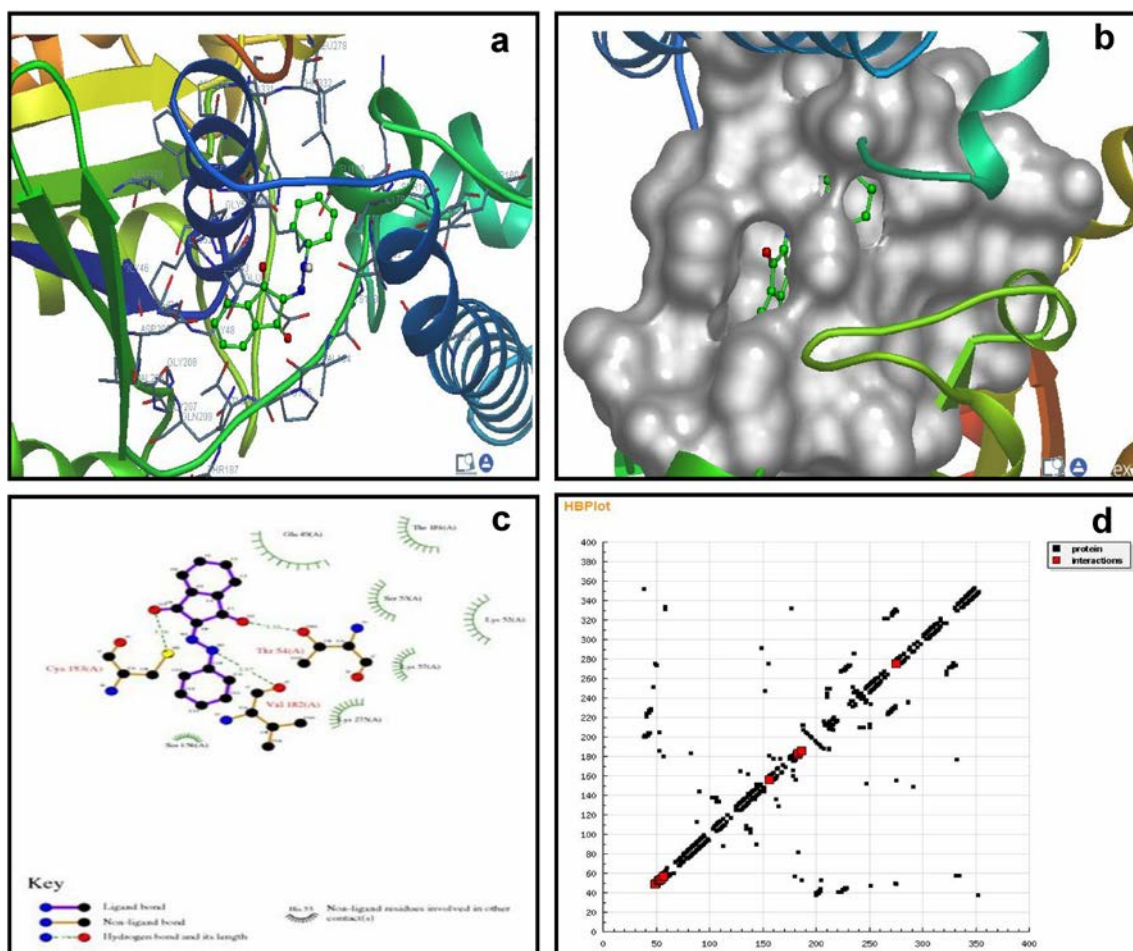


**Fig. S18** Molecular docking studies of compound (1) with 4EKD.

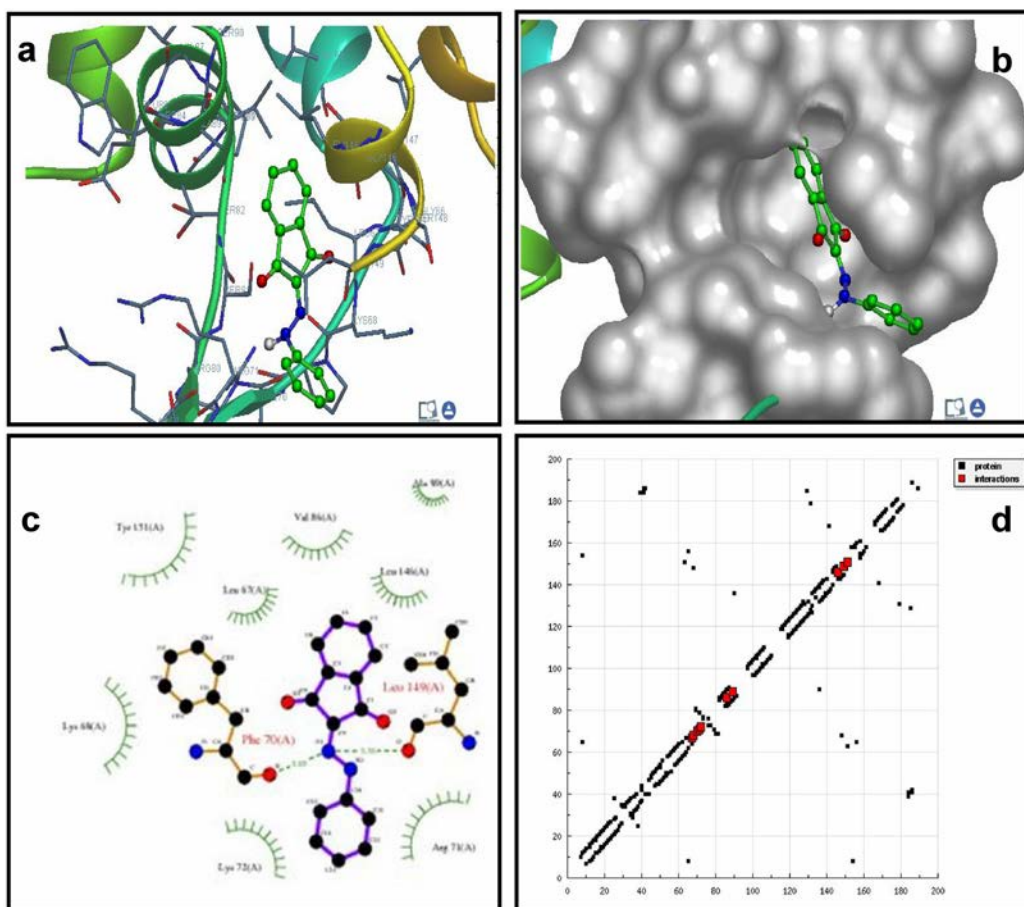


**Fig. S19** Molecular docking studies of compound (1) with 4GIW

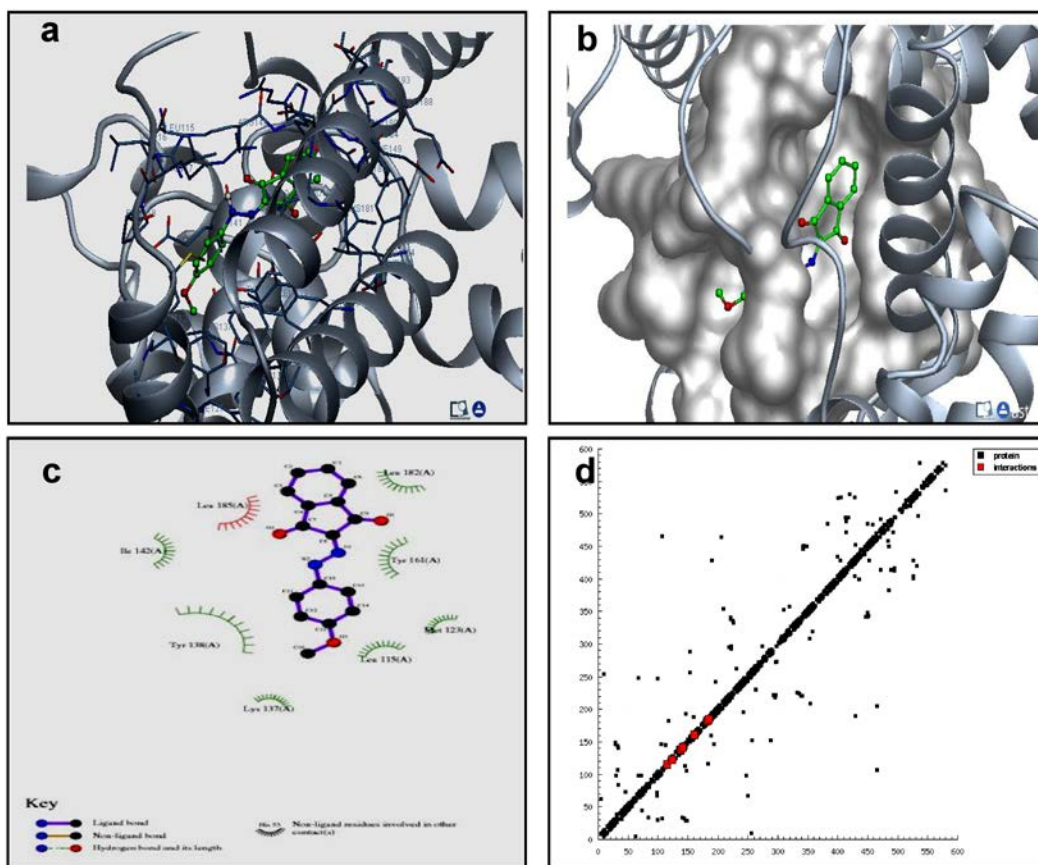


**Fig. S20** Molecular docking studies of compound (2) with 4L9K

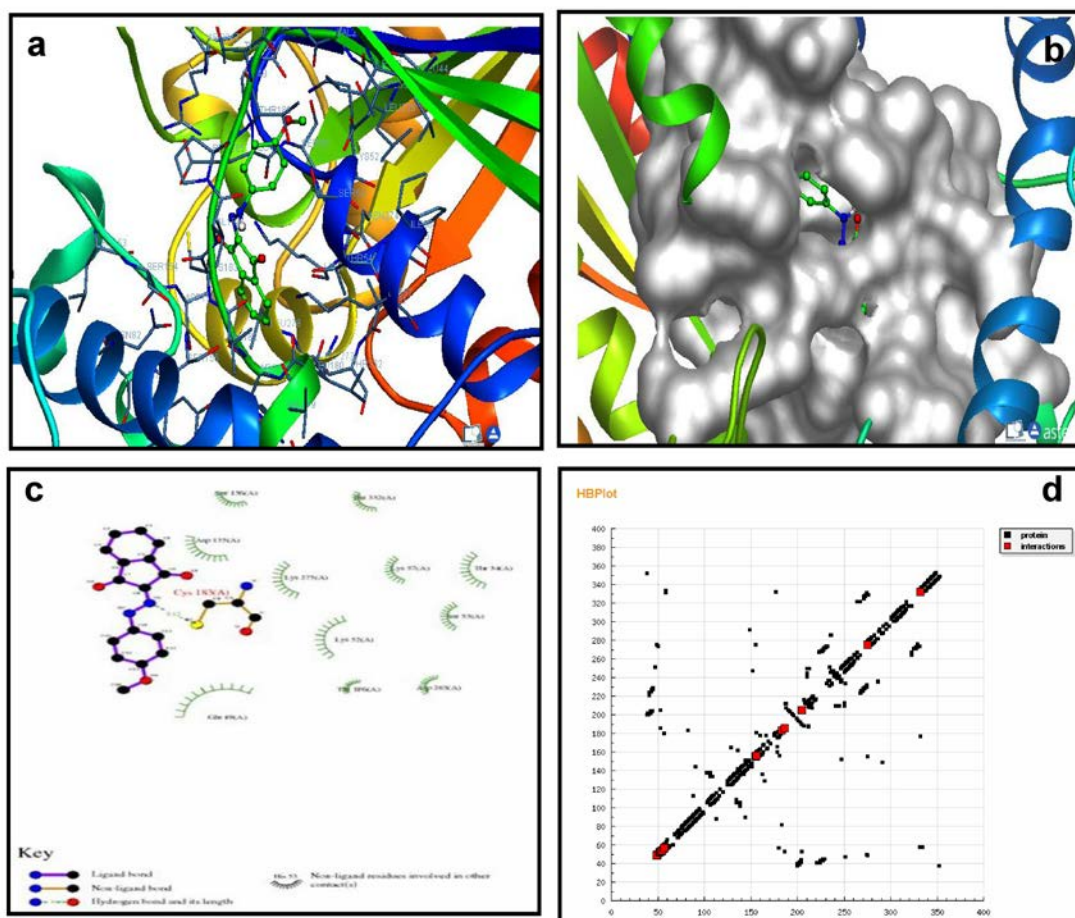


**Fig. S21** Molecular docking studies of compound (2) with 4EKD

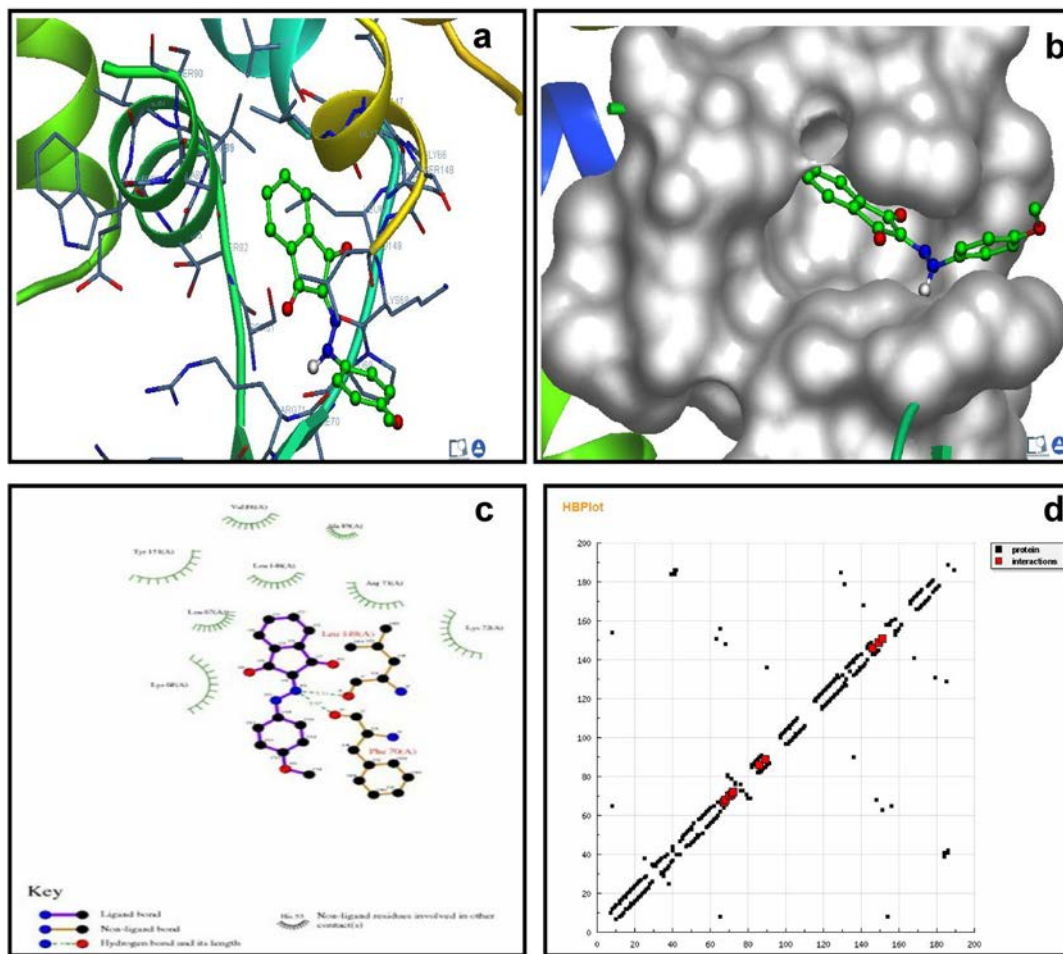


**Fig. S22** Molecular docking studies of compound (2) with 4GIW

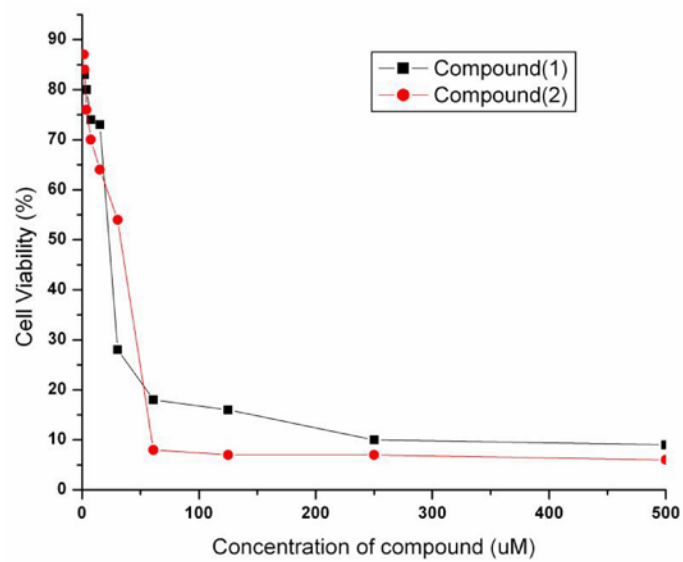


**Fig. S23** Cytotoxic activity of compound (1) and (2) against KB cell line

**Table S1** Absorption and fluorescence values of compound (1) and (2).

S. NO	Solvents	Compound (1)		Compound(2)	
		Absorbance	Fluorescence	Absorbance	Fluorescence
1	Hexane	446	512	400	459
2	1,4-dioxane	447	547	425	459
3	Benzene	449	515	432	479
4	Chloroform	452	512	426	483
5	Ethylacetate	450	516	429	466
6	Dichloromethane	451	499	428	482
7	Acetonitrile	443	546	424	459
8	Ethanol	449	515	425	467
9	2-propanol	449	512	425	459
10	Methanol	446	511	396	484
11	1-hexanol	451	516	428	487
12	2-methylpropane-1-ol	450	514	398	501
13	DMSO	450	519	431	463

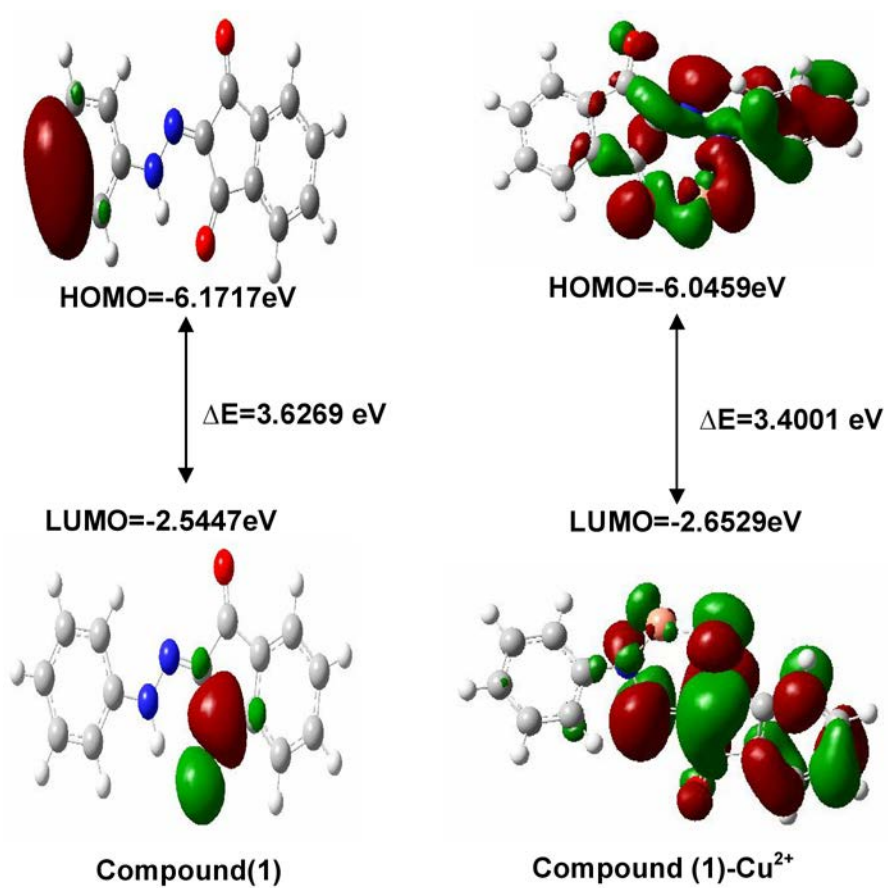


**Fig. S24** HOMO-LUMO energy gap of compound (**1**) with its Cu<sup>2+</sup> complex

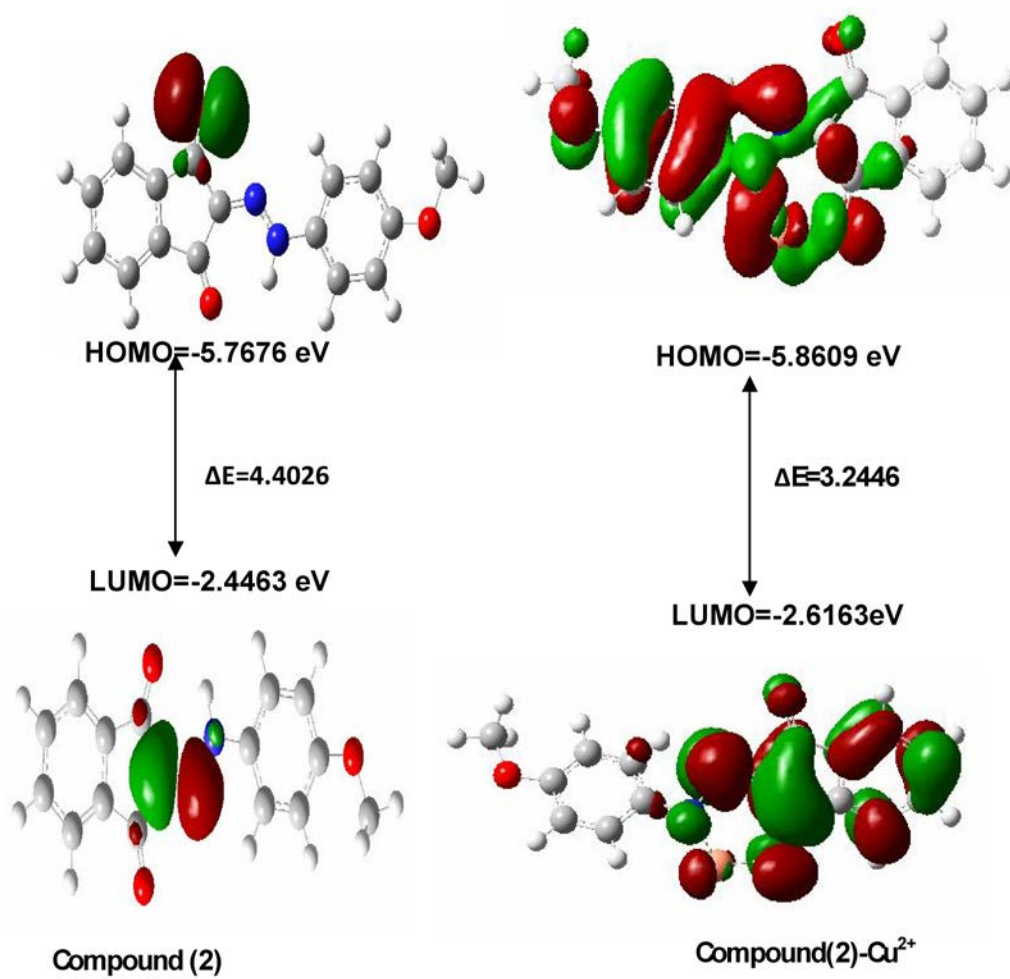
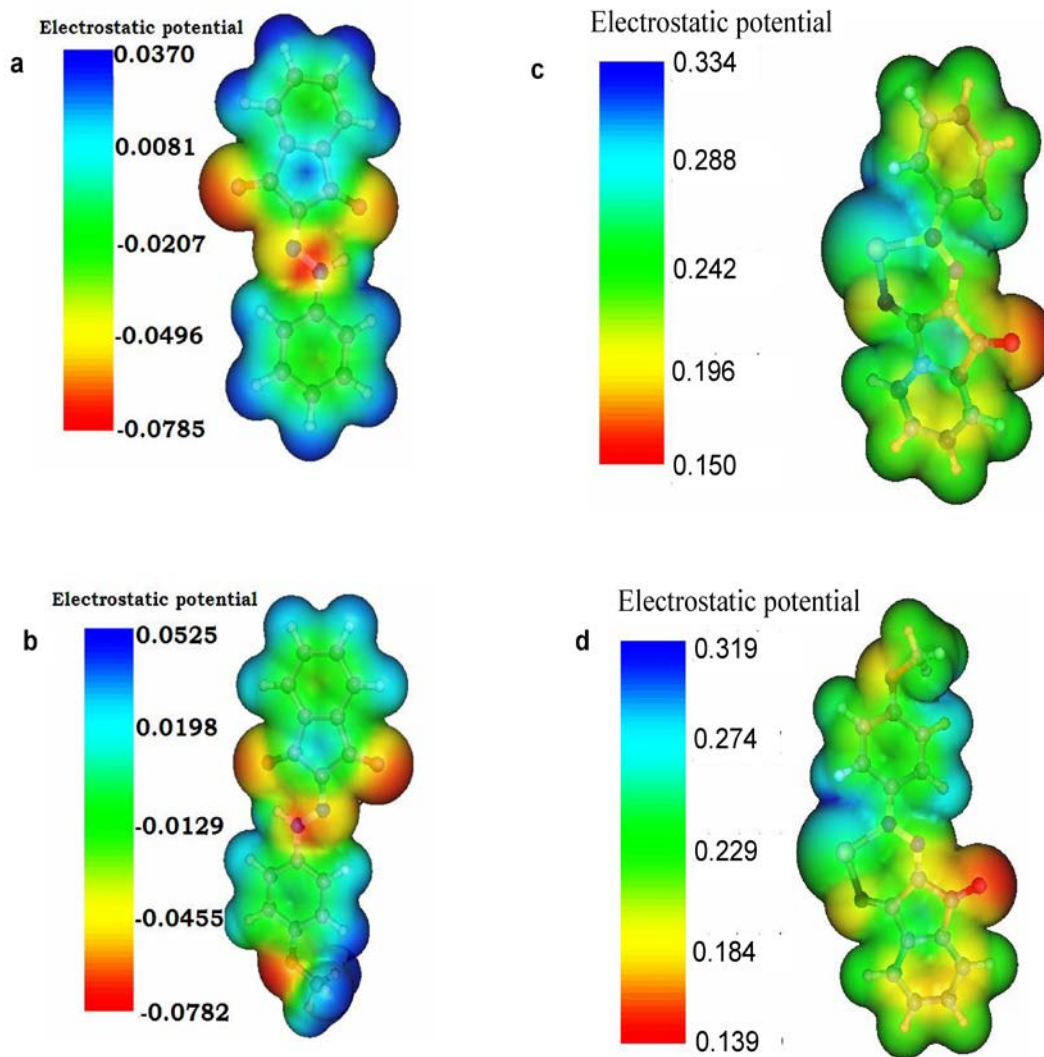


Fig. S25 HOMO-LUMO energy gap of compound (2) with its Cu<sup>2+</sup> complex.



**Fig. S26** Molecular electrostatic potential (MEP) surface of compounds (a and b) (**1**) and (**2**) with  $\text{Cu}^{2+}$  (c and d).

### Molecular electrostatic potential (MEP) maps

To predict reactive sites for electrophilic and nucleophilic attack for the investigated molecule, MEP is calculated (red is negative, blue is positive) at the B3LYP/6-31G and LANL2DZ (d) optimized geometries. Fig. S26a-d show the calculated 3D electrostatic potential contour map of compound (1) and (2) with  $\text{Cu}^{2+}$ . The different values of the electrostatic potential at the surface are represented by different colors. Potential increases in the order red < orange < yellow < green < blue. The color code of these maps is in the range between  $-0.0786 \text{ e}^{-2}$  (deepest red) to  $0.0370 \text{ e}^{-2}$  (deepest blue) in compound (1) and  $-0.0766 \text{ e}^{-2}$  (deepest red) to  $0.0561 \text{ e}^{-2}$  (deepest blue) in compound (2), where blue indicates the strongest attraction and red indicates the strongest repulsion. From this result, it is clear that the H atoms indicate the strongest attraction and O atoms indicate the strongest repulsion in compound (1) and (2). Where as the copper atom indicate the strongest attraction and O atom indicate the repulsion in compound (1) and (2) with  $\text{Cu}^{2+}$  complex.

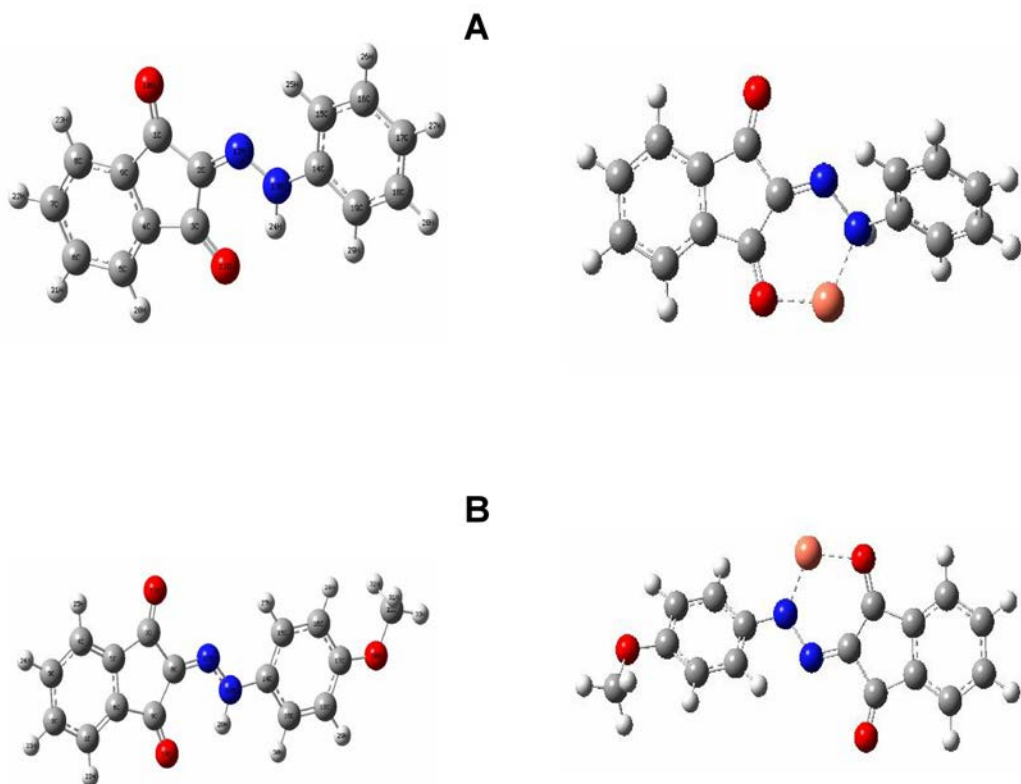


**Fig. S27** Proposed optimized geometries of (A) compound **(1)** (top) and (B) compound **(2)**(Bottom) and its 1 : 1 complex with Cu<sup>2+</sup> ion.

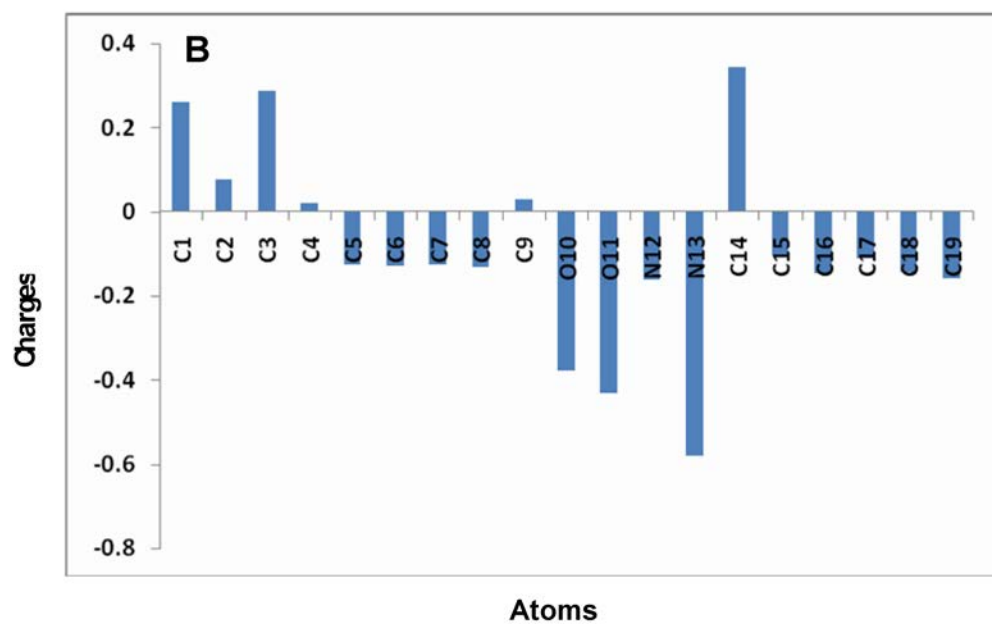
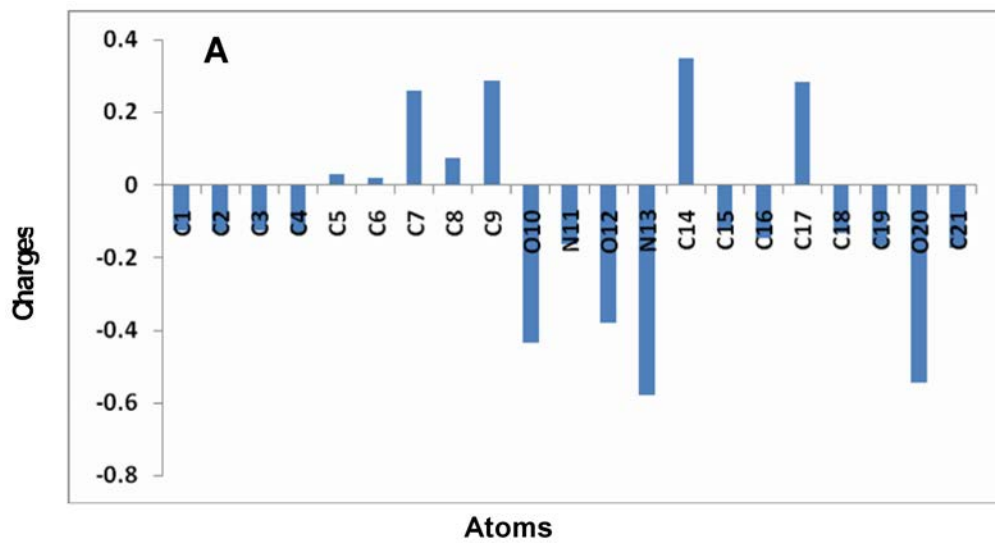


**Fig. S28** Mulliken atomic charges of (A) compound (1) and (B) (2).

## Charge distribution

The charge distribution of the molecule has been calculated on the basis of Mulliken method using a B3LYP/6-31G level calculation. This calculation depicts the charges of the every atom in the molecule. Distribution of positive and negative charges is the vital to increasing or decreasing of bond length between the atoms. Mulliken atomic charges and the plot have shown in Fig. S28. The Mulliken scheme places the negative charge more or less evenly on C5, C7, C8, C10, C11, N12, N13, C15, C16, C17, C18, C19 atoms and C1, C2, C3, C4, O10, N11, O12, N13, C15, C16, C18, O20, C21 atoms in compound (1) and (2) respectively and splits the positive charge among the all hydrogen atom and some of the C1, C2, C3, C4, C9, C14 atoms in (1) and C5, C6, C7, C8, C9, C14, C17 atoms in (2) Mulliken population analysis compute charges by dividing orbital overlap evenly between the two atoms involved.

## References

1. Z. Bikadi and E. Hazai, Application of the PM6 semi-empirical method to modeling proteins enhances docking accuracy of AutoDock, *J. Cheminf.*, 2009, **1**, 15.
2. T. A. Halgren, Merck molecular force field. I. Basis, form, scope, parametrization, and performance of MMFF94, *J. Comput. Chem.*, 1998, **17**, 490.
3. G. M. Morris, D. S. Goodsell, Automated docking using a Lamarckian genetic algorithm and an empirical binding free energy function , *J. Comput. Chem.*, 1998, **19**, 1639.
4. F. J. Solis and R. J. B. Wets Minimization by Random Search Techniques, *Mathematics of Operations Research*, 1981, **6**, 19.